International Journal of Heat and Mass Transfer 52 (2009) 4976–4985

Contents lists available at ScienceDirect

International Journal of Heat and Mass Transfer

journal homepage: www.elsevier.com/locate/ijhmt

Numerical simulation of diffusive processes in solids of revolution via the finite volume method and generalized coordinates

Wilton Pereira da Silva [a], Jürgen W. Precker [a,*], Diogo D.P.S. e Silva [b], Cleiton D.P.S. e Silva [c], Antonio Gilson Barbosa de Lima [d]

[a] Universidade Federal de Campina Grande, Centro de Ciências e Tecnologia, Departamento de Física, Campina Grande, PB, CEP 58109-970, Brazil
[b] Universidade Estadual de Campinas (UNICAMP), Instituto de Matemática, Estatística e Computação Científica, Brazil
[c] Instituto Tecnológico de Aeronáutica (ITA), Divisão de Engenharia Eletrônica (IEE), Brazil
[d] Universidade Federal de Campina Grande, Centro de Ciências e Tecnologia, Unidade Acadêmica de Engenharia Mecânica, Brazil

ARTICLE INFO

Article history:
Received 28 August 2008
Accepted 1 May 2009
Available online 3 July 2009

Keywords:
Diffusive transport
Structured two-dimensional grid
Complex geometries
Drying
Discretization
Fully implicit formulation
Non-orthogonal grids

ABSTRACT

This article proposes a numerical solution of the diffusion equation for solids obtained by revolution of arbitrarily shaped plane surfaces for the description of heat transfer or mass transport. The diffusion equation is discretized and solved using the finite volume method with fully implicit formulation, generalized coordinates and boundary condition of the first kind. The proposed solution exploits symmetry conditions, which reduces the problem to the two-dimensional case, and it diminishes significantly the computational effort in comparison with the traditional method using three-dimensional grids. Our solution is applied to – and compared with – the drying kinetics of solids with known analytical solutions of the diffusion equation. Both solutions agree well in all analyzed cases. Furthermore, our solution is used to describe the moisture distribution inside solids.

1. Introduction

The knowledge of the mechanism of water transfer from the interior of a humid body to an external medium at a given temperature is important for the drying process of a product, because it not only enables to minimize losses of the product, but also the energy consumed during the drying. Naturally, a mathematical model which describes the mechanism of the drying process must be adopted for its theoretical study. Various theories and consequent mathematical models are reported in the literature. One of these assumes, simplifying, that the water transfer from the interior of the product to its surface occurs by liquid diffusion when dried with hot air. Consequently, the appropriate mathematical model to describe the process involves the diffusion equation.

The diffusion equation has an analytical solution for some simple geometries, as for an infinite slab, infinite cylinder, and a sphere, among others. It is normally supposed that these solids have constant thermo-physical properties as, for example, in Ref. [1]. Analytical and numerical solutions for diffusion of water are also reported for parallelepipeds, prolated and oblated spheroids [2–6]. However, only few works are available for arbitrary geometries, particularly using the finite volume method and generalized coordinates. Thus, the study here presented is motivated by the lack of papers involving problems of transient water diffusion in solids of arbitrary geometry, which is necessary for a rigorous description of the drying process of a solid of any shape. In this case, the commonly used Cartesian, cylindrical or spherical coordinates are not appropriate. Even some more flexible coordinate systems, as defined for prolate [2] and oblate [6] spheroids, or still other ellipsoidal systems [7,8], are limited to only some specific geometric shapes, normally involving orthogonal grids.

In this context, our study proposes a numerical solution of the diffusion equation for solids which can be obtained by revolution of arbitrary two-dimensional plane surfaces about a fixed axis in the same plane, thereby exploring symmetry conditions. The proposed numerical solution is for boundary condition of the first kind, using the finite volume method and generalized coordinates, and it can be applied to two-dimensional structured grids, which may be orthogonal or not. Such a study should preview variable physical parameters and enable a description of drying bodies obtained by revolution described above. Our study may be justified by a significant reduction of computational effort in relation to traditional numerical solutions by three-dimensional

* Corresponding author. Tel.: +55 83 3333 3107.
E-mail addresses: wiltonps@uol.com.br (W.P. da Silva), jurgenp@uol.com.br (J.W. Precker), diogodpss@gmail.com (D.D.P.S. e Silva), cleitondiniz@directnet.com.br (C.D.P.S. e Silva), gilson@dem.ufcg.edu.br (A.G.B. de Lima).

0017-9310/$ - see front matter © 2009 Elsevier Ltd. All rights reserved.
doi:10.1016/j.ijheatmasstransfer.2009.05.008

Nomenclature

D	mass diffusivity ($m^2\ s^{-1}$)
J	Jacobian of the transformation (m^{-3})
L	half height of a finite cylinder (m)
M	moisture content (kg/kg), dry basis
$\overline{M}^*$	dimensionless moisture content
r	distance of a nodal point from the axis of revolution (m)
R	radius of a sphere or a finite cylinder (m)
S	source term (dimension depends on the process under study)
t	time in the physical domain

Greek symbols

Γ^{Φ}	transport coefficient (dimension depends on the process under study)
Φ	dependent variable of the diffusion equation (dimension depends on the process under study)
λ	transport coefficient (dimension depends on the process under study)
ξ, η, γ	axes of the system of generalized coordinates (dimensionless)
τ	time in the transformed domain

grids, as in Ref. [9], assuming constant thermo-physical parameters. Besides the presented justification, there is a special interest in this type of solids originating from the great number of industrialized products of this shape and the frequency with which they are found in nature. Although our study was initially motivated by drying problems, it should be noted that the method can be applied to any physical property which can be described by a diffusion equation.

2. Mathematical modelling

The mathematical modelling for the solution of the diffusion equation in the case of drying is based on the following idealizations:

- the solid is considered homogeneous and isotropic;
- the distribution of the moisture content is initially uniform and remains symmetric in relation to the axis of rotation;
- the only mechanism of water transport inside the solid is liquid diffusion;
- the volume of the solid is not affected by the diffusion process.

2.1. Diffusion equation

The diffusion equation in Cartesian coordinates is given by [9–11]

$$\frac{\partial(\lambda\Phi)}{\partial t} = \frac{\partial}{\partial x}\left(\Gamma^{\Phi}\frac{\partial\Phi}{\partial x}\right) + \frac{\partial}{\partial y}\left(\Gamma^{\Phi}\frac{\partial\Phi}{\partial y}\right) + \frac{\partial}{\partial z}\left(\Gamma^{\Phi}\frac{\partial\Phi}{\partial z}\right) + S, \tag{1}$$

where t is the time, x, y and z are the Cartesian coordinates of position, λ and Γ^{Φ} are transport coefficients, S is a source term and Φ is the dependent variable to be determined. Eq. (1) is frequently named diffusion equation of the physical domain, in contrast to the transformed domain.

In general, Cartesian coordinates are not appropriate to solve diffusive problems for solids of arbitrary shape. Thus, a coordinate system whose axes coincide with the borders of the control volume of the studied solid will be used. This means that the new axes, denoted by ξ, η and γ, define a curvilinear, non-orthogonal coordinate system, as shown in Fig. 1.

The curvilinear coordinates ξ, η and γ can be expressed as functions of x, y and z through transformations of the type [10,11]:

$$\xi = \xi(x,y,z); \eta = \eta(x,y,z) \text{ and } \Gamma = \Gamma(x,y,z). \tag{2}$$

Then, the diffusion equation can be written in the new coordinate system as [9,11]:

$$\begin{aligned}\frac{\partial}{\partial\tau}\left(\frac{\lambda\Phi}{J}\right) = {} & \frac{\partial}{\partial\xi}\left(\alpha_{11}J\Gamma^{\Phi}\frac{\partial\Phi}{\partial\xi} + \alpha_{12}J\Gamma^{\Phi}\frac{\partial\Phi}{\partial\eta} + \alpha_{13}J\Gamma^{\Phi}\frac{\partial\Phi}{\partial\Gamma}\right) \\ & + \frac{\partial}{\partial\eta}\left(\alpha_{21}J\Gamma^{\Phi}\frac{\partial\Phi}{\partial\xi} + \alpha_{22}J\Gamma^{\Phi}\frac{\partial\Phi}{\partial\eta} + \alpha_{23}J\Gamma^{\Phi}\frac{\partial\Phi}{\partial\Gamma}\right) \\ & + \frac{\partial}{\partial\Gamma}\left(\alpha_{31}J\Gamma^{\Phi}\frac{\partial\Phi}{\partial\xi} + \alpha_{32}J\Gamma^{\Phi}\frac{\partial\Phi}{\partial\eta} + \alpha_{33}J\Gamma^{\Phi}\frac{\partial\Phi}{\partial\Gamma}\right) + \frac{S}{J},\end{aligned} \tag{3}$$

where τ is the time, and J is the Jacobian of the transformation to be defined below, together with the coefficients α_{ij} for the type of solid under study. Eq. (3), written in generalized coordinates ξ, η and γ, is frequently called diffusion equation in the transformed domain. Note that the structured grid to be used in Eq. (3) is fixed in time, i.e., the volume of the solid is constant.

2.2. Diffusion equation for solids of revolution

The solution proposed in this paper for solids of revolution is similar to that for diffusion in long solids obtained by extrusion (see, for example, Ref. [11]). But a solution via the finite volume method for non-orthogonal two-dimensional structured grids in an arbitrary domain and generalized coordinates was not found in the consulted literature. The basic idea departs from a control volume generated by an elementary cell of a two-dimensional structured grid in the (x, y)-plane through rotation by an angle θ about y, as sketched in Fig. 2. Since a symmetric diffusion in relation to the y-axis is assumed, there is no flux in the direction of γ perpendicular to the generating cell of the control volume.

The derivatives of x and y with respect to γ, and the derivatives of z with respect to ξ and η, are zero for the control volume shown in Fig. 2. In this case, the generating cell is contained in the vertical (ξ, η)-plane, while γ and z lie in a horizontal plane. Thus, the Jacobian of the transformation is given by the determinant

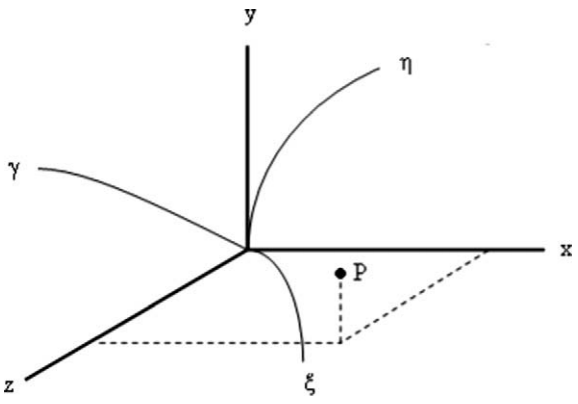

Fig. 1. Cartesian and generalized coordinate systems.

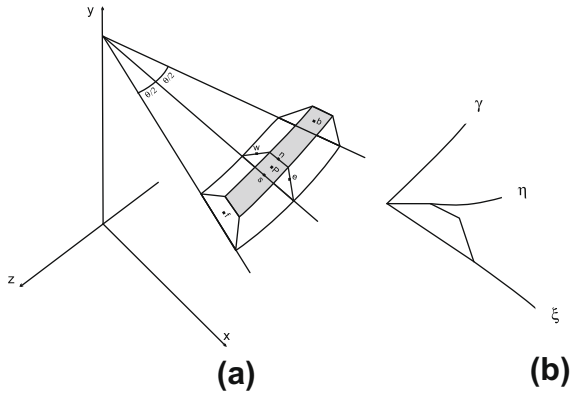

Fig. 2. (a) Control volume with a nodal point P obtained by rotation about y of an elementary cell of a two-dimensional structured grid in a vertical plane. The faces "f" and "b" refer to front and back. (b) System of generalized coordinates defined by the axes ξ, η and γ along the borders of the control volume.

$$\frac{1}{J}=\begin{vmatrix} x_\xi & x_\eta & 0 \\ y_\xi & y_\eta & 0 \\ 0 & 0 & z_\gamma \end{vmatrix}, \tag{4}$$

or

$$\frac{1}{J}=z_\gamma\begin{vmatrix} x_\xi & x_\eta \\ y_\xi & y_\eta \end{vmatrix}, \tag{5}$$

where the symbol g_m means the partial derivative of g with respect to m. Therefore, for a solid of revolution, the Jaobian is given by the 2×2 determinant of Eq. (5), instead of the 3×3 determinant of Eq. (4).

Since there is no flux in the direction of γ for the solid of revolution under study, the third term of the right hand side of Eq. (3) becomes zero, because a derivative with respect to γ is involved. By hypothesis, the derivative of Φ with respect to γ is also zero. In this case, Eq. (3) turns into

$$\frac{\partial}{\partial\tau}\left(\frac{\lambda\Phi}{J}\right)=\frac{\partial}{\partial\xi}\left(\alpha_{11}J\Gamma^{\Phi}\frac{\partial\Phi}{\partial\xi}+\alpha_{12}J\Gamma^{\Phi}\frac{\partial\Phi}{\partial\eta}\right)+\frac{\partial}{\partial\eta}\left(\alpha_{21}J\Gamma^{\Phi}\frac{\partial\Phi}{\partial\xi}+\alpha_{22}J\Gamma^{\Phi}\frac{\partial\Phi}{\partial\eta}\right), \tag{6}$$

and the 3D diffusion problem (ξ, η and γ) is transformed into a 2D one (ξ and η). Thus, besides the knowledge of the Jacobian determined by Eq. (5), the following expressions must be known for the numeric solution of Eq. (6):

$$\alpha_{11}=z_\gamma^2(x_\eta^2+y_\eta^2);\quad \alpha_{12}=\alpha_{21}=-z_\gamma^2(x_\xi x_\eta+y_\xi y_\eta);\quad \alpha_{22}=z_\gamma^2(x_\xi^2+y_\xi^2). \tag{7a-c}$$

Obviously, the terms α_{13}, α_{31}, α_{23}, α_{32} and α_{33}, which are related to the γ -axis, need not be calculated for a solid of revolution. Moreover, a parallelepiped (3D-case), discretized in the transformed domain, transforms into a rectangle (2D-case) as will be shown below using the finite volume method.

The principal difference between a 2D solution for solids of revolution, as proposed in this article, and a typical 2D solution for solids obtained by extrusion of plane areas along the z-axis, is the form how z_γ is calculated. In the latter case, $z_\gamma = 1$ because $z=\gamma$, whereas for the proposed solution for solids of revolution z_γ is obtained as will be defined by Eq. (10).

2.3. Numerical solution: discretization of the diffusion equation

With fully implicit formulation, integration of Eq. (6) about space and time for a solid of revolution gives for a control volume with elementary cell in the (ξ,η)-plane and unit length in γ for a time interval $\Delta\tau$:

$$\begin{aligned}\frac{\lambda_P\Phi_P-\lambda_P^0\Phi_P^0}{J_P}\Delta\xi\Delta\eta=&\left[\alpha_{11e}J_e\Gamma_e^{\Phi}\Delta\eta\Delta\tau\frac{\partial\Phi}{\partial\xi}\Big|_e+\alpha_{12e}J_e\Gamma_e^{\Phi}\Delta\eta\Delta\tau\frac{\partial\Phi}{\partial\eta}\Big|_e\right]\\&-\left[\alpha_{11w}J_w\Gamma_w^{\Phi}\Delta\eta\Delta\tau\frac{\partial\Phi}{\partial\xi}\Big|_w+\alpha_{12w}J_w\Gamma_w^{\Phi}\Delta\eta\Delta\tau\frac{\partial\Phi}{\partial\eta}\Big|_w\right]\\&+\left[\alpha_{21n}J_n\Gamma_n^{\Phi}\Delta\xi\Delta\tau\frac{\partial\Phi}{\partial\xi}\Big|_n+\alpha_{22n}J_n\Gamma_n^{\Phi}\Delta\xi\Delta\tau\frac{\partial\Phi}{\partial\eta}\Big|_n\right]\\&-\left[\alpha_{21s}J_s\Gamma_s^{\Phi}\Delta\xi\Delta\tau\frac{\partial\Phi}{\partial\xi}\Big|_s+\alpha_{22s}J_s\Gamma_s^{\Phi}\Delta\xi\Delta\tau\frac{\partial\Phi}{\partial\eta}\Big|_s\right]\\&+\frac{S_P}{J_P}\Delta\xi\Delta\eta\Delta\tau,\end{aligned} \tag{8}$$

where the terms without superscript are evaluated at time $\tau+\Delta\tau$, while the terms with superscript zero are evaluated at a previous time τ. The subscripts "e", "w", "n" and "s" mean the east, west, north and south borders, respectively, of an elementary cell of a control volume of unit length, while P is the nodal point of this volume. All the elements described above are shown in Fig. 2.

To complete the discretization of Eq. (8), it should be noted that for a structured two-dimensional grid created in the generating plane surface of the solid of revolution, there are nine types of different control volumes in the transformed domain, as shown in Fig. 3.

Obviously, each type of control volume shown in Fig. 3 generates a distinct algebraic equation originating from the discretization of Eq. (8). As can be observed in Eq. (8), the term J must be calculated at the nodal point P of each control volume and also, as well as α_{11}, α_{12} or α_{21} and α_{22}, at the east, west, north and south borders of the elementary cell which defines that volume. As the expressions for J, α_{11}, α_{12} or α_{21} and α_{22} depend on the derivatives x_ξ, y_ξ, x_η, y_η and z_γ, the knowledge of the expressions for these derivatives for the solid of revolution is necessary.

2.4. Internal control volume

The derivatives of the coordinates x and y with respect to ξ and η for the nodal point of an internal control volume of a grid can be obtained from the fragment of the grid of the transformed domain shown in Fig. 4.

As can be deduced from Fig. 4, the metric for the nodal point P relative to the transformations of the domains are given by the following expressions:

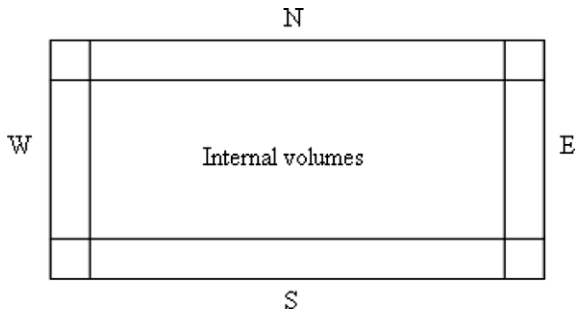

Fig. 3. Regions with nine types of control volumes in the transformed domain for a structured grid: internal volumes, and boundary volumes in the north (N), in the south (S), in the east (E) and in the west (W).

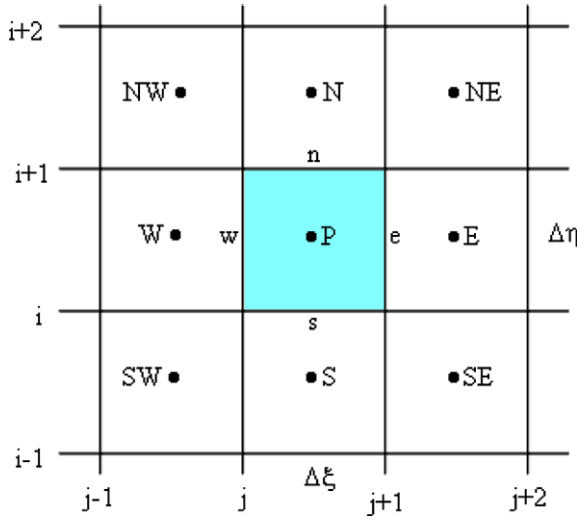

Fig. 4. Internal control volume P and its neighbours in the north (N), south (S), east (E), west (W), north-east (NE), north-west (NW), south-east (SE) and south-west (SW).

$$
\begin{aligned}
x^P_\xi &= \frac{x_e - x_w}{\Delta\xi} = \left[\frac{x_{i,j+1}+x_{i+1,j+1}}{2} - \frac{x_{i,j}+x_{i+1,j}}{2}\right]\cdot\frac{1}{\Delta\xi}\\
x^P_\eta &= \frac{x_n - x_s}{\Delta\eta} = \left[\frac{x_{i+1,j}+x_{i+1,j+1}}{2} - \frac{x_{i,j}+x_{i,j+1}}{2}\right]\cdot\frac{1}{\Delta\eta},\\
y^P_\xi &= \frac{y_e - y_w}{\Delta\xi} = \left[\frac{y_{i,j+1}+y_{i+1,j+1}}{2} - \frac{y_{i,j}+y_{i+1,j}}{2}\right]\cdot\frac{1}{\Delta\xi},\\
y^P_\eta &= \frac{y_n - y_s}{\Delta\eta} = \left[\frac{y_{i+1,j}+y_{i+1,j+1}}{2} - \frac{y_{i,j}+y_{i,j+1}}{2}\right]\cdot\frac{1}{\Delta\eta},
\end{aligned}
\tag{9a-d}
$$

where the indices i and j determine the positions of the η and ξ lines which delimit the elementary cell of the generating two-dimensional grid of the solid of revolution. Further, the derivative of z with respect to γ is given by:

$$
z^P_\gamma = \frac{z^P_f - z^P_b}{\Delta\gamma} = \theta r\frac{1}{\Delta\gamma},
\tag{10}
$$

where the indices "f" and "b" refer to front and back, respectively, as can be observed in Fig. 2. On the other hand, r is the distance from the axis of revolution to the nodal point, calculated by

$$
r = \frac{x_{ij}+x_{i,j+1}+x_{i+1,j+1}+x_{i+1,j}}{4}.
\tag{11}
$$

For solids of revolution as considered in this article, the metric z^P_γ, given by Eq. (10), is determined by the value of r (distance from P to the y-axis, see Fig. 2). On the other hand, r is localized in the vertical plane (ξ,η) or (x,y), and its value only depends on the x coordinate as is evident from Eq. (11).

For the east border of an internal control volume, the derivatives of the coordinates x and y with respect to ξ and η are given by the equations:

$$
\begin{aligned}
x^e_\xi &= \left[\frac{x_{i,j+2}+x_{i+1,j+2}}{2} - \frac{x_{i,j}+x_{i+1,j}}{2}\right]\cdot\frac{1}{2\Delta\xi},\\
x^e_\eta &= \frac{x_{i+1,j+1}-x_{i,j+1}}{\Delta\eta},\\
y^e_\xi &= \left[\frac{y_{i,j+2}+y_{i+1,j+2}}{2} - \frac{y_{i,j}+y_{i+1,j}}{2}\right]\cdot\frac{1}{2\Delta\xi},\\
y^e_\eta &= \frac{y_{i+1,j+1}-y_{i,j+1}}{\Delta\eta},
\end{aligned}
\tag{12a-d}
$$

whereas the derivative of z with respect to γ is also given by Eq. (10), but r becomes now:

$$
r = \frac{x_{i,j+1}+x_{i+1,j+1}}{2}.
\tag{13}
$$

With similar expressions to those obtained above, all necessary terms for a complete definition of α_{11}, α_{12} or α_{21}, α_{22} and J for the north, south and west borders of an internal control volume can be determined.

For an internal control volume, the derivatives of Φ in Eq. (8) can be approximated as:

$$
\begin{aligned}
&\left.\frac{\partial\Phi}{\partial\xi}\right|_e = \frac{\Phi_E-\Phi_P}{\Delta\xi};\left.\frac{\partial\Phi}{\partial\eta}\right|_e = \frac{\Phi_N+\Phi_{NE}-\Phi_S-\Phi_{SE}}{4\Delta\eta};\left.\frac{\partial\Phi}{\partial\xi}\right|_w = \frac{\Phi_P-\Phi_W}{\Delta\xi};\\
&\left.\frac{\partial\Phi}{\partial\eta}\right|_w = \frac{\Phi_N+\Phi_{NW}-\Phi_S-\Phi_{SW}}{4\Delta\eta};\left.\frac{\partial\Phi}{\partial\xi}\right|_n = \frac{\Phi_E+\Phi_{NE}-\Phi_W-\Phi_{NW}}{4\Delta\xi};\\
&\left.\frac{\partial\Phi}{\partial\eta}\right|_n = \frac{\Phi_N-\Phi_P}{\Delta\eta};\left.\frac{\partial\Phi}{\partial\xi}\right|_s = \frac{\Phi_E+\Phi_{SE}-\Phi_W-\Phi_{SW}}{4\Delta\xi};\left.\frac{\partial\Phi}{\partial\eta}\right|_s = \frac{\Phi_P-\Phi_S}{\Delta\eta}.
\end{aligned}
\tag{14a-h}
$$

So, finally, the discretization of Eq. (8) for an internal control volume results in the following algebraic equation:

$$
\begin{aligned}
A_p\Phi_P = {} & A_w\Phi_W + A_e\Phi_E + A_s\Phi_S + A_n\Phi_N + A_{sw}\Phi_{SW} + A_{se}\Phi_{SE}\\
& + A_{nw}\Phi_{NW} + A_{ne}\Phi_{NE} + B,
\end{aligned}
\tag{15}
$$

where:

$$
\begin{aligned}
A_P &= \frac{\lambda_P}{J_P}\cdot\frac{\Delta\xi\Delta\eta}{\Delta\tau} + \alpha_{11e}J_e\Gamma^\Phi_e\frac{\Delta\eta}{\Delta\xi} + \alpha_{11w}J_w\Gamma^\Phi_w\frac{\Delta\eta}{\Delta\xi}\\
&\quad + \alpha_{22n}J_n\Gamma^\Phi_n\frac{\Delta\xi}{\Delta\eta} + \alpha_{22s}J_s\Gamma^\Phi_s\frac{\Delta\xi}{\Delta\eta}\\
A_w &= \alpha_{11w}J_w\Gamma^\Phi_w\frac{\Delta\eta}{\Delta\xi} + \frac{1}{4}\alpha_{21s}J_s\Gamma^\Phi_s - \frac{1}{4}\alpha_{21n}J_n\Gamma^\Phi_n\\
A_e &= \alpha_{11e}J_e\Gamma^\Phi_e\frac{\Delta\eta}{\Delta\xi} + \frac{1}{4}\alpha_{21n}J_n\Gamma^\Phi_n - \frac{1}{4}\alpha_{21s}J_s\Gamma^\Phi_s\\
A_s &= \alpha_{22s}J_s\Gamma^\Phi_s\frac{\Delta\xi}{\Delta\eta} + \frac{1}{4}\alpha_{12w}J_w\Gamma^\Phi_w - \frac{1}{4}\alpha_{12e}J_e\Gamma^\Phi_e\\
A_n &= \alpha_{22n}J_n\Gamma^\Phi_n\frac{\Delta\xi}{\Delta\eta} + \frac{1}{4}\alpha_{12e}J_e\Gamma^\Phi_e - \frac{1}{4}\alpha_{12w}J_w\Gamma^\Phi_w\\
A_{sw} &= \frac{1}{4}\alpha_{12w}J_w\Gamma^\Phi_w + \frac{1}{4}\alpha_{21s}J_s\Gamma^\Phi_s\\
A_{se} &= -\frac{1}{4}\alpha_{12e}J_e\Gamma^\Phi_e - \frac{1}{4}\alpha_{21s}J_s\Gamma^\Phi_s\\
A_{nw} &= -\frac{1}{4}\alpha_{12w}J_w\Gamma^\Phi_w - \frac{1}{4}\alpha_{21n}J_n\Gamma^\Phi_n\\
A_{ne} &= \frac{1}{4}\alpha_{12e}J_e\Gamma^\Phi_e + \frac{1}{4}\alpha_{21n}J_n\Gamma^\Phi_n\\
B &= \frac{\lambda^0_P\Phi^0_P}{J_P}\cdot\frac{\Delta\xi\Delta\eta}{\Delta\tau} + \frac{S_P}{J_P}\Delta\xi\Delta\eta
\end{aligned}
\tag{16a-j}
$$

Commonly, the ξ and η lines of a grid in the transformed domain are identified by consecutive integers, and therefore as well $\Delta\xi$ as $\Delta\eta$ are equal to 1 in Eq. (16) and in the other equations in which they appear.

2.5. Dirichlet boundary condition

With an analogue procedure as presented for the internal control volumes of a grid, the algebraic equations can be determined for every type of control volume identified in Fig. 3. For example, Fig. 5 shows control volumes at the east boundary of a fragment of a two-dimensional grid in the transformed domain.

For a nodal point P in the control volume at the east boundary shown in Fig. 5, and assuming boundary condition of the first kind, one obtains:

$$
A_p\Phi_P = A_w\Phi_W + A_s\Phi_S + A_n\Phi_N + A_{sw}\Phi_{SW} + A_{nw}\Phi_{NW} + B,
\tag{17}
$$

where

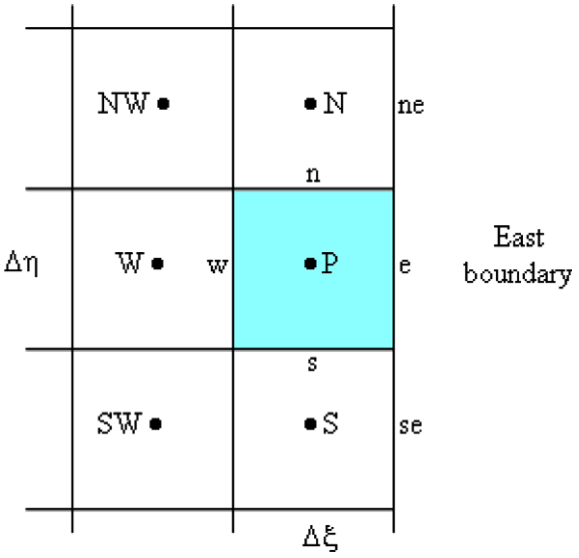

Fig. 5. Control volume P at the east boundary and its neighbours.

$$
\begin{aligned}
A_p &= \frac{\lambda_P}{J_P}\cdot\frac{\Delta\xi\Delta\eta}{\Delta\tau} + 2\alpha_{11e}J_e\Gamma^{\Phi}_e\frac{\Delta\eta}{\Delta\xi} + \alpha_{11w}J_w\Gamma^{\Phi}_w\frac{\Delta\eta}{\Delta\xi} \\
&\quad + \alpha_{22n}J_n\Gamma^{\Phi}_n\frac{\Delta\xi}{\Delta\eta} + \alpha_{22s}J_s\Gamma^{\Phi}_s\frac{\Delta\xi}{\Delta\eta} + \frac{1}{4}\alpha_{21n}J_n\Gamma^{\Phi}_n - \frac{1}{4}\alpha_{21s}J_s\Gamma^{\Phi}_s, \\
A_w &= \alpha_{11w}J_w\Gamma^{\Phi}_w\frac{\Delta\eta}{\Delta\xi} + \frac{1}{4}\alpha_{21s}J_s\Gamma^{\Phi}_s - \frac{1}{4}\alpha_{21n}J_n\Gamma^{\Phi}_n, \\
A_s &= \alpha_{22s}J_s\Gamma^{\Phi}_s\frac{\Delta\xi}{\Delta\eta} + \frac{1}{4}\alpha_{21s}J_s\Gamma^{\Phi}_s + \frac{1}{4}\alpha_{12w}J_w\Gamma^{\Phi}_w, \\
A_n &= \alpha_{22n}J_n\Gamma^{\Phi}_n\frac{\Delta\xi}{\Delta\eta} - \frac{1}{4}\alpha_{21n}J_n\Gamma^{\Phi}_n - \frac{1}{4}\alpha_{12w}J_w\Gamma^{\Phi}_w, \\
A_{sw} &= \frac{1}{4}\alpha_{21s}J_s\Gamma^{\Phi}_s + \frac{1}{4}\alpha_{12w}J_w\Gamma^{\Phi}_w, \\
A_{nw} &= -\frac{1}{4}\alpha_{21n}J_n\Gamma^{\Phi}_n - \frac{1}{4}\alpha_{12w}J_w\Gamma^{\Phi}_w, \\
B &= \frac{\lambda^0_P\Phi^0_P}{J_P}\cdot\frac{\Delta\xi\Delta\eta}{\Delta\tau} + \frac{S_P}{J_P}\Delta\xi\Delta\eta + 2\alpha_{11e}J_e\Gamma^{\Phi}_e\frac{\Delta\eta}{\Delta\xi}\Phi_e + \frac{1}{2}\alpha_{12e}J_e\Gamma^{\Phi}_e(\Phi_{ne}-\Phi_{se}) \\
&\quad + \frac{1}{2}\alpha_{21n}J_n\Gamma^{\Phi}_n(\Phi_{ne}+\Phi_e) - \frac{1}{2}\alpha_{21s}J_s\Gamma^{\Phi}_s(\Phi_{se}+\Phi_e),
\end{aligned}
\tag{18a-g}
$$

and Φ_e, Φ_{ne} and Φ_{se} are the values of Φ at the east, north-east and south-east boundaries, respectively, as shown in Fig. 5.

It should be noted that for the case of a control volume at the east boundary, the derivatives for the determination of α_{11}, α_{12} or α_{21}, α_{22} and J are the same as used for an internal control volume, with the exception of x^e_ξ and y^e_ξ. These last two derivatives can be approximated by x^p_ξ and y^p_ξ, respectively. Similar approximations can be made for each of the other borders of the cell: north, south and west.

2.6. Symmetry

To exploit possible simplifications caused by symmetries, as presented in this article, boundary condition without flux may be useful. If such a boundary condition is applied to the east boundary, for example, the discretized diffusion equation for a control volume becomes:

$$A_p\Phi_P = A_w\Phi_W + A_s\Phi_S + A_n\Phi_N + A_{sw}\Phi_{SW} + A_{nw}\Phi_{NW} + B, \tag{19}$$

where

$$
\begin{aligned}
A_P &= \frac{\lambda_P}{J_P}\cdot\frac{\Delta\xi\Delta\eta}{\Delta\tau} + \alpha_{11w}J_w\Gamma^{\Phi}_w\frac{\Delta\eta}{\Delta\xi} - \frac{1}{4}\alpha_{21n}J_n\Gamma^{\Phi}_n + \alpha_{22n}J_n\Gamma^{\Phi}_n\frac{\Delta\xi}{\Delta\eta} \\
&\quad + \frac{1}{4}\alpha_{21s}J_s\Gamma^{\Phi}_s + \alpha_{22s}J_s\Gamma^{\Phi}_s\frac{\Delta\xi}{\Delta\eta}, \\
A_w &= \alpha_{11w}J_w\Gamma^{\Phi}_w\frac{\Delta\eta}{\Delta\xi} + \frac{1}{4}\alpha_{21s}J_s\Gamma^{\Phi}_s - \frac{1}{4}\alpha_{21n}J_n\Gamma^{\Phi}_n, \\
A_s &= \alpha_{22s}J_s\Gamma^{\Phi}_s\frac{\Delta\xi}{\Delta\eta} + \frac{1}{4}\alpha_{12w}J_w\Gamma^{\Phi}_w - \frac{1}{4}\alpha_{21s}J_s\Gamma^{\Phi}_s, \\
A_n &= \alpha_{22n}J_n\Gamma^{\Phi}_n\frac{\Delta\xi}{\Delta\eta} + \frac{1}{4}\alpha_{21n}J_n\Gamma^{\Phi}_n - \frac{1}{4}\alpha_{12w}J_w\Gamma^{\Phi}_w, \\
A_{sw} &= \frac{1}{4}\alpha_{12w}J_w\Gamma^{\Phi}_w + \frac{1}{4}\alpha_{21s}J_s\Gamma^{\Phi}_s, \\
A_{nw} &= -\frac{1}{4}\alpha_{12w}J_w\Gamma^{\Phi}_w - \frac{1}{4}\alpha_{21n}J_n\Gamma^{\Phi}_n, \\
B &= \frac{\lambda^0_P\Phi^0_P}{J_P}\cdot\frac{\Delta\xi\Delta\eta}{\Delta\tau} + \frac{S_P}{J_P}\Delta\xi\Delta\eta.
\end{aligned}
\tag{20a-g}
$$

Similar equations as above can be written for the other types of control volumes, and a system of equations in Φ is obtained which can be solved, for example, by the method of Gauss–Seidel.

Note that the proposed solution for solids of revolution may also be used for typical two-dimensional diffusion (long solids obtained by extrusion) imposing $z_\gamma = 1$, instead of Eq. (10). Finally should be mentioned that the here presented numerical solution presupposes the general case involving a non-orthogonal grid, and therefore the so called cross-terms ($A_{sw}\Phi_{SW}$, $A_{se}\Phi_{SE}$, $A_{nw}\Phi_{NW}$ and $A_{ne}\Phi_{NE}$) appear in the calculations, which would not happen for an orthogonal grid.

2.7. Mean value of Φ

If the values of Φ are known for each control volume at time t, its mean value can be determined by the equation [12,14]

$$\overline{\Phi} = \frac{1}{V}\int \Phi dV \tag{21}$$

or, with the appropriate discretization [14]

$$\overline{\Phi} = \frac{1}{\sum\frac{1}{J_P}}\sum\Phi_P\frac{1}{J_P}, \tag{22}$$

where the summation must be applied over all control volumes. The term $1/J_P$ corresponds to the volume of the control volume containing the nodal point P. Hence, the mean value of Φ is determined by a weighted mean in which the volume of each control volume is used for the weighting.

2.8. Variable coefficient Γ^{Φ}

In the case of a variable transport coefficient Γ^{Φ}, a harmonic mean will be used for its estimation at the borders of each control volume [13,14]. For example, for the border "e" between a control volume with a nodal point P and its east neighbour with nodal point E (see Fig. 4), one obtains:

$$\Gamma^{\Phi}_e = \frac{\Gamma^{\Phi}_P\Gamma^{\Phi}_E}{f_d\Gamma^{\Phi}_E + (1-f_d)\Gamma^{\Phi}_P}, \tag{23}$$

where

$$f_d = \frac{d_P}{d_P + d_E}, \tag{24}$$

and d_P and d_E are the distances from the border "e" to the nodal points P and E, respectively. At the nodal points, Γ^{Φ} must be calculated by an appropriate function which relates Γ^{Φ} with the value of Φ at each node.

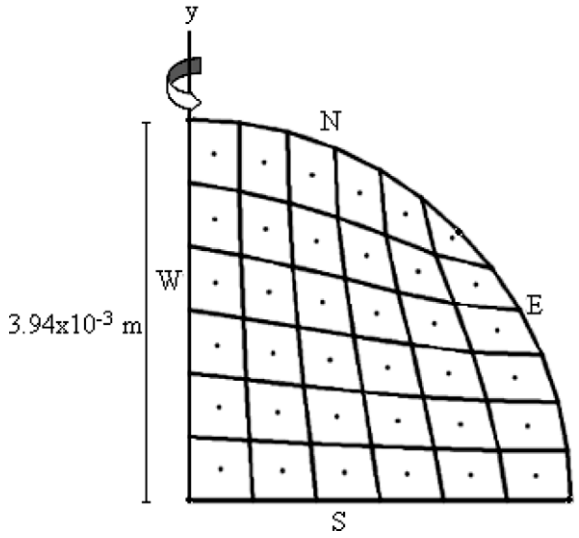

Fig. 6. Initial 6 × 6 grid for a quarter of the circle ($r = 3.94 \times 10^{-3}$ m), highlighting the nodes of the generating cells of the control volumes and the boundaries.

So, for each time step, we have a system of equations which will be solved by Gauss–Seidel, with a tolerance of 10^{-8}.

The proposed numerical solution can be used to study the conduction of heat if we impose: $\Phi = T$ (temperature), $\Gamma^{\Phi} = k$ (conductivity) and $\lambda = \rho c_p$ (ρ is the density and c_p is the specific heat). On the other hand, setting $\Phi = M$ (moisture content), $\Gamma^{\Phi} = D$ (water diffusivity), $\lambda = 1$, and $S = 0$, the proposed numerical solution can be used to study the water diffusion in solids.

The software employed in this work (including user interface) was developed in Compaq Visual Fortran Professional Edition V. 6.6.0 (Fortran 95) using a programming language option called QuickWin Application, under Windows XP platform.

3. Results and discussion

Many tests have been made to evaluate the numerical solution proposed in this paper, and the results obtained are available in Ref. [14]. Out of these, three simulations concerning drying of porous solids will be presented in the following, as examples which serve to validate the proposed solution. For the case of diffusion of water in porous media, the parameter λ of Eq. (6) should be set equal to 1, Γ^{Φ} represents the effective mass diffusivity D, and the dependent variable Φ is the moisture content M.

3.1. Example 1: sphere with constant diffusivity

The first example describes thin-layer drying of cowpea using air at 40 °C, and all data used in this example were extracted from Ref. [15]. This example, besides to enable a description of the drying kinetic of cowpea by the proposed numerical solution, also allows validating the solution if non-orthogonal grids are used, and therefore cross-terms make part of the solution. With regard to the data, the grains are idealized as spheres with a radius of 3.94×10^{-3} m. For the proposed numerical solution, the sphere is obtained by revolution of a quarter of a circle about the y-axis, as shown in Fig. 6. The grid was generated by the software 2D Grid Generation[1].

The initial and boundary conditions, as well as the properties of the solid, are defined as follows:

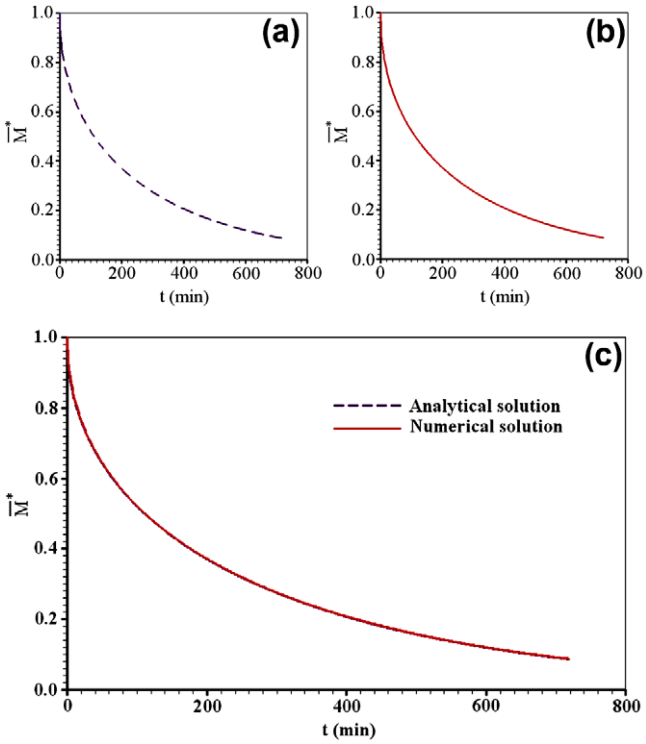

Fig. 7. Dimensionless average moisture content of cowpea as a function of time: (a) Analytical solution; (b) Proposed numerical solution; (c) Superposition of the two solutions.

- initial condition:

uniform initial moisture content in the domain: $M_i = 0.59$ kg/kg (db, dry basis);

- boundary conditions:

$M = M_{eq} = 0.088$ kg/kg, db at the curved boundary of Fig. 6 (north and east);

$-D\frac{\partial M}{\partial n} = 0$, at west and south (no flux of water), being n the normal direction at the boundaries.

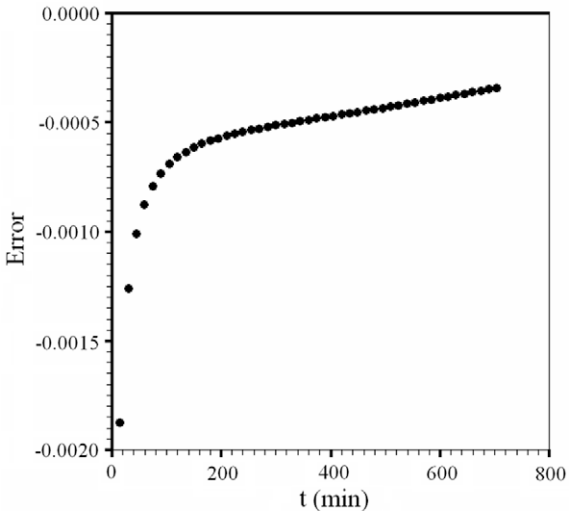

Fig. 8. Residual error as a function of time.

[1] http://zeus.df.ufcg.edu.br/labfit/gg.htm, accessed on April 2008.

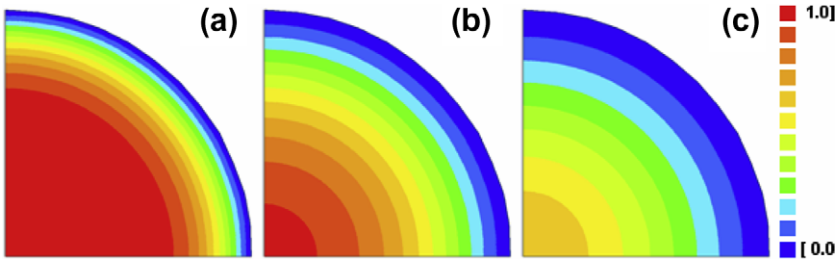

Fig. 9. Contour plots showing the moisture content of the generating area of the cowpea grain at t = : (a) 50 min; (b) 200 min; (c) 400 min.

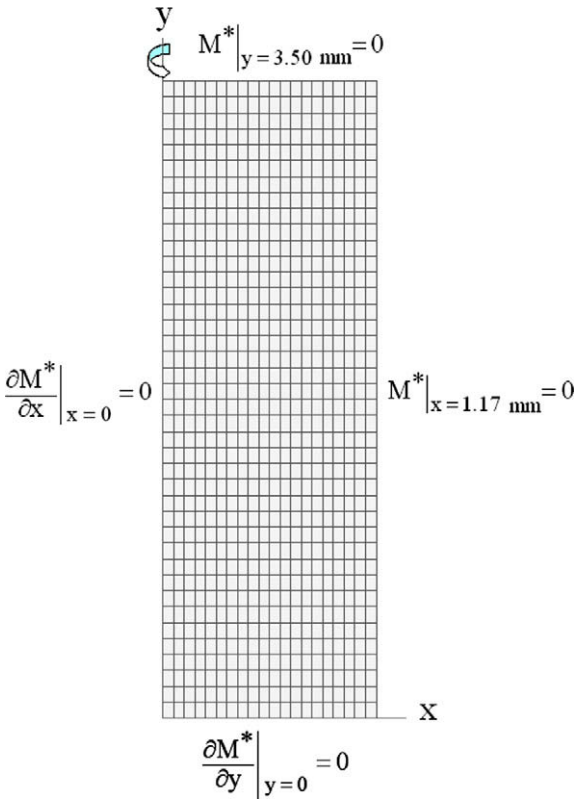

Fig. 10. Grid of the generating rectangle for the cylindrical model of rice grains. The value of 3.50 mm corresponds to the half height of the cylinder and the value of 1.17 mm corresponds to the radius.

- properties of the medium:

constant effective mass diffusivity $D = 7.13 \times 10^{-11}\ \mathrm{m^2\ s^{-1}}$ ($D = 4.28 \times 10^{-9}\ \mathrm{m^2\ min^{-1}}$) and $\lambda = 1$.

For the problem under investigation, without source term and with prescribed boundary condition, the analytical solution for the average moisture content $\overline{M}$ is given by [1]

$$\overline{M}^{*} = \frac{\overline{M} - \overline{M}_{eq}}{\overline{M}_i - \overline{M}_{eq}} = \frac{6}{\pi^2} \sum_{n=1}^{\infty} \frac{1}{n^2} \exp\left(-n^2 \frac{\pi^2}{R^2} Dt\right), \tag{25}$$

where $\overline{M}_{eq}$ is the average value of M at equilibrium, and $\overline{M}^{*}$ is the dimensionless moisture content.

The time of drying was 720 min, studies of time and grid refinement indicated an interval of $\Delta t = 30$ s and a grid with 48×48 generating cells of the control volumes, considering a tolerance of 1×10^{-3} of the dimensionless moisture content.

Fig. 7a shows the dimensionless average moisture content as a function of time obtained from the analytical solution using 40 terms of the series of Eq. (25). Fig. 7b shows the result of the proposed numerical solution, and Fig. 7c the superposition of both.

Fig. 7 indicates complete agreement of the analytical solution obtained from Eq. (25) with the numerical solution proposed in this paper for transient diffusion in a sphere. To get an idea of the discrepancy between the two solutions, we consider the residual error defined as

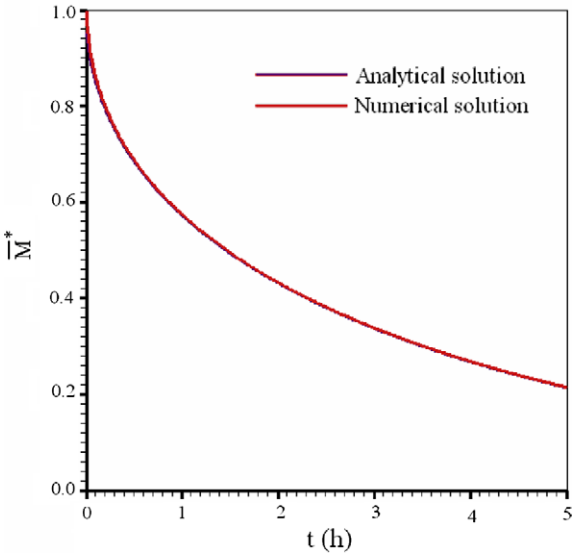

Fig. 11. Drying kinetic of rice. Comparison of the analytical and numerical solution.

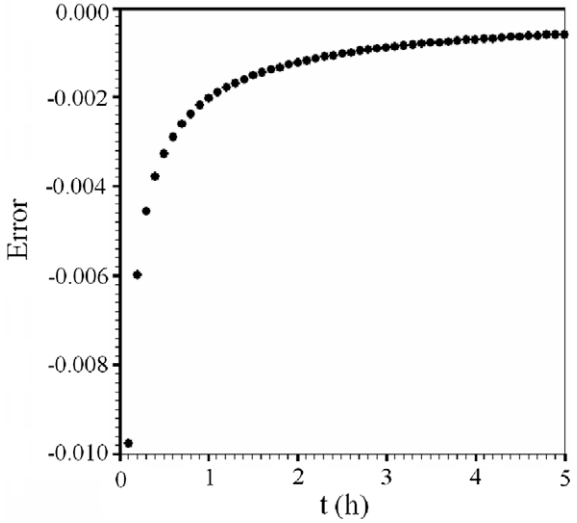

Fig. 12. Residual error as a function of drying time.

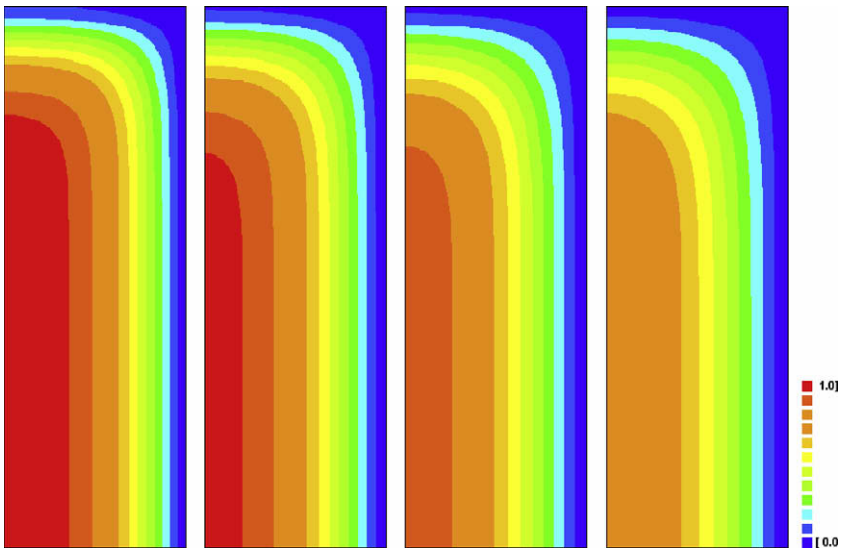

Fig. 13. Contour plots of the drying process at the instants: 1.5; 2.0; 2.5 and 3.0 h.

$$\text{Error} = \overline{M}^{*}_{\text{analytical}} - \overline{M}^{*}_{\text{numerical}}. \tag{26}$$

Fig. 8 shows the residual error as a function of time.

We conclude from Fig. 8 that the numerical solution agrees with the analytical solution within the tolerance of 1×10^{-3}, which had been imposed for the studies of time and grid refinement. Note further that the calculation of the analytical solution included only the first 40 terms of the series.

The proposed numerical solution has the advantage to be more general than the analytical one, because it can be applied to any solid obtained by revolution of an arbitrary plane surface. Moreover, the numerical solution allows simulations with variable process parameters. Finally, the evolution of the spatial distribution of the moisture content with time can be visualized, as shown in Fig. 9 for the sphere under investigation.

As can be observed in Fig. 9, the moisture content decreases more rapidly in the region near the surface than in the interior at the beginning of the drying process. This means that greater moisture content gradients are present in the region near the surface, and therefore effects due to internal tensions may there occur during the drying process.

3.2. Example 2: finite cylinder with constant diffusivity

This example is extracted from Ref. [12], and describes thin-layer drying of rice by the model of liquid diffusion, starting from experimental data. The rice (each grain is considered as a finite cylinder) was dried by air at 60 °C flowing with a velocity of 1.5 m s^{-1}. The drying kinetic was described by the analytical solution of a finite cylinder. We will compare that solution with the numerical solution proposed in this paper.

For the numerical simulation, the total time of the drying process was divided into 1000 equal intervals. A 20×40 grid was created in a rectangle with dimensions of 1.17×3.50 mm which is the generating area of the cylinder representing the rice grain, as shown in Fig. 10. The boundary conditions, exploiting the symmetries of the problem, are also shown.

Besides describing the drying kinetic of rice, this example allows to validate the proposed numerical solution when orthogonal grids are used, what implies that the cross-terms are equal to zero. Note that in this case the transformation of the 3D-problem into a 2D-problem by rotation of the grid about an axis could be developed using Cartesian coordinates.

The analytical solution of the problem is given by [12,16]

$$\overline{M}^{*} = \frac{\overline{M} - \overline{M}_{eq}}{\overline{M}_i - \overline{M}_{eq}} = \sum_{n=1}^{\infty}\sum_{m=1}^{\infty} \frac{8}{\alpha_n^2 \beta_m^2} \exp\left[-\left(\alpha_n^2 + \beta_m^2 \frac{R^2}{L^2}\right)\frac{Dt}{R^2}\right], \tag{27}$$

where α_n are the roots of the Bessel functions of the first kind and order zero, $\beta_m = (2m-1)\pi/2$, L is the half height of the finite cylinder, and R is its radius. The result of the analytical solution for a diffusivity $D = 1.3224 \times 10^{-11}$ m^2 s^{-1} ($D = 4.7608 \times 10^{-8}$ m^2 h^{-1}), and initially uniform moisture content ($M_i^* = 1$), calculated from Eq. (25) for $n = 30$ and $m = 1000$, is shown in Fig. 11. The numerical solution proposed in this paper is also shown for comparison.

Fig. 12 shows the residual error as a function of time.

The numerical solution permits to preview the distribution of the moisture content inside the grains at selected times, as shown in Fig. 13 by contour plots.

3.3. Example 3: finite cylinder with variable diffusivity

To get an idea of how well the liquid-diffusion model with constant diffusivity matches experimental data for the drying kinetic of rice, the results of the foregoing example are plotted together with experimental data in Fig. 14. The data referring to 60 °C have been extracted from Ref. [12] and digitalized using the software xyExtract Graph digitizer[2]. The figure contains the statistical fitting indicators chi-squared (χ^2) and the determination coefficient (R^2) [17,18], determined by LAB Fit Curve Fitting Software [19].

As can be seen from Fig. 14, the liquid-diffusion model with boundary condition of the first kind and constant diffusivity does not adequately describe the initial instants of the drying. At the beginning of the drying process the diffusivity should be somewhat less than 1.3224×10^{-11} m^2 s^{-1} (4.7608×10^{-8} m^2 h^{-1}), whereas its value should be slightly higher at the end of the drying. Thus, to relate the diffusivity with the local moisture content, simulations were carried out with various decreasing functions and, analysing the statistical indicators of all realized fits, we propose that the dependence of the diffusivity on local moisture content may be described by an expression of the form

$$D = \frac{B}{\cosh(AM^{*2})}. \tag{28}$$

[2] http://zeus.df.ufcg.edu.br/labfit/index_xyExtract.htm, accessed on April 2008.

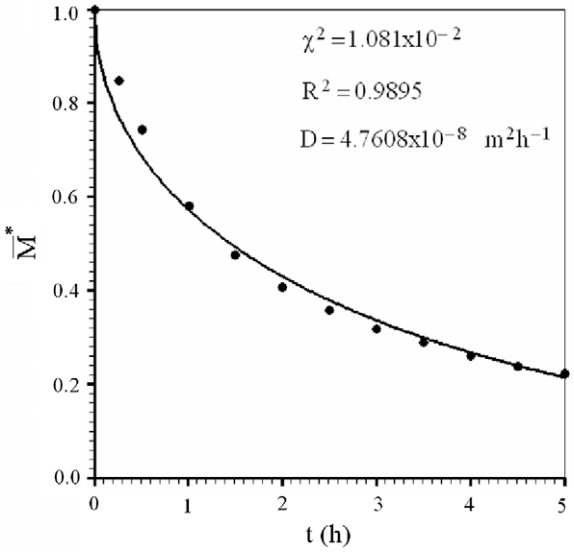

Fig. 14. Drying kinetic of rice at 60 °C assuming constant diffusivity.

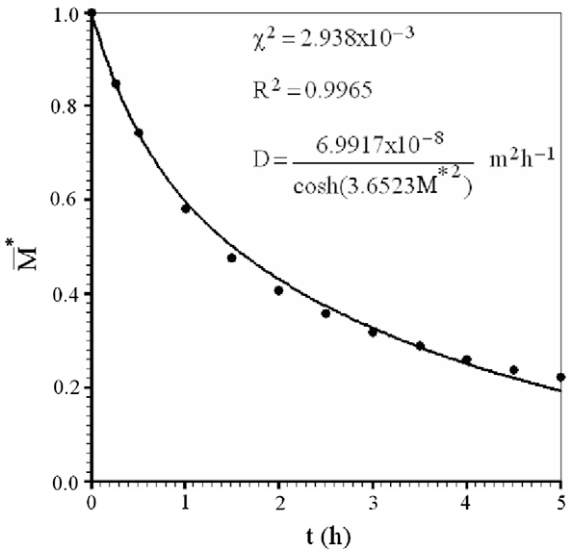

Fig. 15. Drying kinetic of rice assuming variable diffusivity given by Eq. (28).

The values of $A = 3.6523$ and $B = 1.9421 \times 10^{-11}\ m^2\ s^{-1}$ ($B = 6.9917 \times 10^{-8}\ m^2\ h^{-1}$) were calculated by the method of inverse optimization [20]. In the inverse method, values are assigned to the parameters of interest, the equation which describes the system is solved, and the results are compared to the experimental data relative to the system. After comparison, new values for the parameters are established followed by a new solution and the process continues until the results satisfactorily agree with the experimental data. This method has been used to obtain the drying kinetic of Fig. 15.

Comparison of the statistical indicators of Figs. 14 and 15 shows that the numerical simulation of the drying kinetic of rice with variable diffusivity matches the experimental data better than a simulation with constant diffusivity. Fig. 16 shows the decreasing diffusivity as a function of the local moisture content.

In examples 1, 2 and 3, we use in our article the same boundary condition as the original papers, from which the data were obtained. Naturally, if the boundary condition of the first kind is not completely acceptable to describe a drying process, the obtained diffusivity only should be interpreted as an expression that fits the numerical simulation to the experimental data. On the other hand should be observed that for the convective boundary condition, with increasing moisture content, increasing diffusivities are expected [21–24], and not the opposite, as obtained in this article for a boundary condition of first kind.

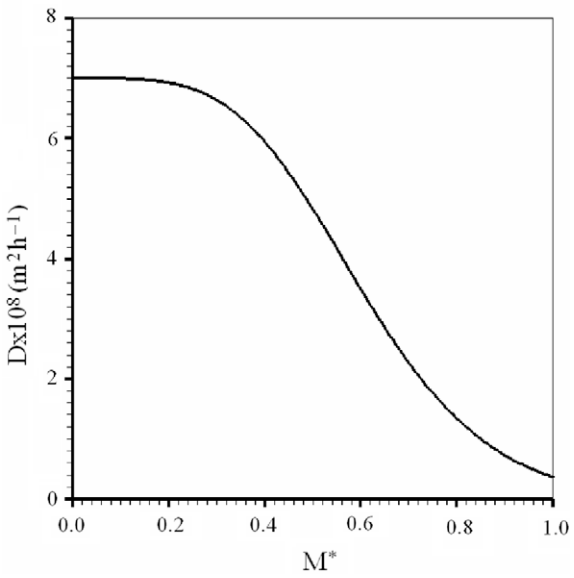

Fig. 16. Diffusivity as a function of the local moisture content given by Eq. (28).

With regard to the validation of the proposed method for solids of revolution via the finite volume method and generalized coordinates, it can be verified by example 1 that the numerical solution produces correct results for non-orthogonal grids. Example 2 shows that the proposed numerical solution also produces correct results for orthogonal grids. Finally, as example 3 reveals, the proposed solution is also useful for the solution of diffusive problems with a variable diffusivity.

4. Conclusions

The numerical solution for the diffusion equation in solids of revolution, subject to boundary condition of the first kind, proposed in this work, produces compatible results with the results expected for all tests carried out. This means that diffusion in such solids can be studied starting from two-dimensional grids, which simplifies the numerical solution of this type of problems and reduces the computational effort in comparison with typical three-dimensional solutions. In addition, differently from the analytical solutions presented, the numerical solution makes available the spatial distribution of the moisture content at any instant. Thus, it is possible to analyze gradients of moisture content and foresee possible problems regarding the drying process at a given temperature.

The numerical solution proposed in this article can also be used for a simulation of diffusion in long solids obtained by extrusion, setting $z_\gamma = 1$. In this sense, the proposed solution represents a generalization of the typical two-dimensional solution available in the literature using the finite volume method.

The proposed solution permits to establish an expression for the diffusivity as a function of local moisture content, which is an advantage in relation to other solutions assuming constant diffusivity.

The numerical solution proposed in this article can not only be applied to mass transfer, but also to other diffusive problems. For example, in the case of heat conduction, the parameter λ must be

substituted by ρc_p, where ρ is the density of the solid and c_p its specific heat at constant pressure, while Γ^{Φ} must be substituted by the thermal conductivity k.

Acknowledgements

We acknowledge partial financial support of this work by the Brazilian organizations CAPES (Coordenação de Aperfeiçoamento de Pessoal de Nível Superior) and CNPq (Conselho Nacional de Desenvolvimento Científico e Tecnológico).

References

[1] J. Crank, The Mathematics of Diffusion, Clarendon Press, Oxford, UK, 1992.
[2] A.G.B. Lima, Fenômeno de difusão em sólidos esferoidais prolatos. Estudo de caso: secagem de banana, Tese de Doutorado, Universidade Estadual de Campinas, São Paulo, Brasil, 1999.
[3] C. Jia, W. Yang, T.J. Siebenmorgen, A.G. Cnossen, Development of computer simulation software for single grain kernel drying, tempering and stress analysis, in: Proceedings of the Annual International Meeting, Sacramento, California, 2001, ASAE paper number 01-3010.
[4] J.J.S. Nascimento, Fenômenos de difusão transiente em sólidos paralelepípedos. Estudo de caso: secagem de materiais cerâmicos, Tese de Doutorado, Universidade Federal da Paraíba, João Pessoa, PB, Brasil, 2002.
[5] D.R. Lima, S. N Farias, A.G. B Lima, Mass transport in spheroids using the Galerkin method, Braz. J. Chem. Eng. 21 (4) (2004) 667–680.
[6] J.E.F. Carmo, Fenômeno de difusão transiente em sólidos esferoidais oblatos. Estudo de caso: secagem de lentilhas, Tese de Doutorado, Universidade Federal de Campina Grande, PB, Brasil, 2004.
[7] Z. Li, N. Kobayashi, M. Hasatani, Modeling of diffusion in ellipsoidal solids: a comparative study, Drying Technol. 22 (4) (2004) 649–675.
[8] A.L. Gastón, R.M. Abalone, S.A. Giner, D.M. Bruce, Geometry effect on water diffusivity estimation in printa-isla verde and broom wheat cultivars, Latin Am. Appl. Res. 33 (1) (2003) 327–331 (Bahía Blanca).
[9] B. Wu, W. Yang, C. Jia, A three-dimensional numerical simulation of transient heat and mass transfer inside a single rice kernel during the drying process, Biosyst. Eng. 87 (2) (2004) 191–200.
[10] J.C. Tannehill, D.A. Anderson, R.H. Pletcher, Computational Fluid Mechanics and Heat Transfer, second ed., Taylor & Francis, Philadelphia, 1997.
[11] C.R. Maliska, Transferência de calor e mecânica dos fluidos computacional, LTC Editora S.A., Rio de Janeiro, 2004.
[12] O. Hacihafizoglu, A. Cihan, K. Kahveci, A.G.B. Lima, A liquid diffusion model for thin-layer drying of rough rice, Eur. Food Res. Technol. (2007), doi: 10.1007/s00217-007-0593-0.
[13] S.V. Patankar, Numerical Heat Transfer and Fluid Flow, Hemisphere Publishing Corporation, New York, 1980.
[14] W.P. Silva, Transporte difusivo em sólidos com forma arbitrária usando coordenadas generalizadas, Tese de Doutorado, Universidade Federal de Campina Grande, PB, Brasil, 2007.
[15] W.P. Silva, M.E.R.M. Cavalcanti Mata, C.D.P.S.e. Silva, M.A. Guedes, A.G.B. Lima, Determination of diffusivity and activation energy for cowpea grains (*vigna unguiculata* (l.) *walp.*), always-green variety, based on its drying behavior, Eng. Agríc. 28 (2) (2008) 325–333.
[16] A.V. Luikov, Analytical Heat Diffusion Theory, Academic Press, Inc. Ltd, London, 1968.
[17] P.R. Bevington, D.K. Robinson, Data Reduction and Error Analysis for the Physical Sciences, second ed., WCB/McGraw-Hill, Boston, 1992.
[18] J.R. Taylor, An Introduction to Error Analysis, second ed., University Science Books, Sausalito, California, 1997.
[19] W.P. Silva, C.D.P.S.e Silva, LAB Fit Curve Fitting Software. Available from: <www.labfit.net> (accessed on April 2008).
[20] V.C. Mariani, A.G.B. Lima, L.S. Coelho, Apparent thermal diffusivity estimation of the banana during drying using inverse method, J. Food Eng. 85 (4) (2008) 569–579.
[21] C.T. Kiranoudis, Z.B. Maroulis, D. Marinos-Kouris, Heat and mass transfer model building in drying with multiresponse data, Int. J. Heat Mass Transfer 38 (3) (1995) 463–480.
[22] N.P. Zogzas, Z.B. Maroulis, Effective Moisture diffusivity estimation from drying data – a comparison between various methods of analysis, Drying Technol. 14 (7) (1996) 1543–1573.
[23] N. Hamdami, J.Y. Monteau, A. Le Bail, Transport properties of a high porosity model food at above and sub-freezing temperatures. Part 2: evaluation of the effective moisture diffusivity from drying data, J. Food Eng. 62 (4) (2004) 385–392.
[24] I.I. Ruiz-López, M.A. García-Alvarado, Analytical solution for food-drying kinetics considering shrinkage and variable diffusivity, J. Food Eng. 79 (1) (2007) 208–216.